Growth of small diameter multi-walled carbon nanotubes by arc discharge process

K. T. Chaudhary[a)†], J. Ali[a)], and P. P. Yupapin[b)]

[a)] *Institute of Advanced Photonics Science (APSI), Nanotechnology Research Alliance, Universiti Teknologi Malaysia* 81310, *Johor Bahru, Malaysia*
[b)] *Nanoscale Science and Research Alliance (N'SERA), Faculty of Science, King Mongkut's Institute of Technology Ladkrabang, Bangkok* 10520, *Thailand*

(Received 24 June 2013; revised manuscript received 13 July 2013; published online 24 January 2014)

Multi-walled carbon nanotubes (MWCNTs) are grown by arc discharge method in a controlled methane environment. The arc discharge is produced between two graphite electrodes at the ambient pressures of 100 torr, 300 torr, and 500 torr. Arc plasma parameters such as temperature and density are estimated to investigate the influences of the ambient pressure and the contributions of the ambient pressure to the growth and the structure of the nanotubes. The plasma temperature and density are observed to increase with the increase in the methane ambient pressure. The samples of MWCNT synthesized at different ambient pressures are analyzed using transmission electron microscopy, scanning electron microscopy, Raman spectroscopy, Fourier transform infrared spectroscopy, and X-ray diffraction. An increase in the growth of MWCNT and a decrease in the inner tube diameter are observed with the increase in the methane ambient pressure.

Keywords: electric discharge, arc plasma temperature and density, carbon nanotubes

PACS: 52.80.–s, 52.25.–b, 81.07.–b **DOI:** 10.1088/1674-1056/23/3/035203

1. Introduction

Carbon nanotubes and nanostructures have great potential and incredible versatility[1,2] for different technological applications, such as nano electronic devices,[3,4] fuel cells, purification and filtering systems, sensors,[5] data storage, bio-engineering applications,[6] nanomaterials, and composites,[7] due to the uniqueness of their geometries and structures.[1] Arc discharge plasma is used extensively in a variety of applications, such as surface modification, micro and nano fabrication, thin film deposition, ion implantation, sources of particles and radiations (ions, electrons, excited atoms, radicle, molecules, x-rays, etc).[8–11] It is also a simple and effective technique to grow high quality nanotube structures[12] compared with the other techniques such as chemical vapor deposition[13–15] and laser ablation.[16] The arc discharge is a versatile technique suitable for the large-scale production of high-quality carbon nanotubes.[17] The high influx of carbon species in arc plasma provides a suitable environment for the growth and development of nanotubes and nanostructures.[3,18,19] However, the main obstacle is the lack of control of growth and less understanding of the growth mechanisms of nanotubes and structures during arc discharge.[1,12] To realize the full potential and for optimized applications, the controlled and selective growth of carbon nanotubes and nanostructures is the basic requirement.[13] For the optimized growth and better understanding of the growth mechanism, the influences of the experimental parameters including residence gas, background pressure, applied voltage and current, electromagnetic field, electrode dimension,[20] etc. on the product need to be explored.[21] The growth of nanostructures during arc discharge depends not only on the ambient environment but also on the dynamics of the carbon species. Thus, understanding the kinematics of carbon species and the role of ambient gas pressure in the nucleation of nanostructures is of great importance.[22]

In this paper, the growth of a multi-walled carbon nanotube (MWCNT) is investigated with methane serving as the background and feedstock gas. The contributions of the methane (CH_4) ambient pressure to the structural geometry of growing MWCNT and to the plasma dynamics are discussed.

2. Experimental procedure

The MWCNTs are synthesized by arc discharge generated between two 5N (99.999%) pure graphite electrodes in a controlled CH_4 environment. The graphite rods with diameters of 11 mm and 9 mm are used as the cathode and the anode, respectively. The discharge is carried out at a dc arc current of 90 A for CH_4 ambient pressures 100 torr, 300 torr, and 500 torr. The plasma temperature and density are determined by optical emission spectroscopy. The optical emission spectra are recorded under each experimental condition by focusing the radiation from the carbon discharge plasma onto the optical fiber connected to the optical spectrometer using a bi-convex lens. The grown structures of MWCNTs are collected from the cathode surface and subjected to analysis by transmission electron microscopy (TEM), scanning electron microscopy (SEM), x-ray diffraction (XRD), Raman spectroscopy, and Fourier transform infrared (FTIR) spectroscopy.

†Corresponding author. E-mail: kashif.ali02@gmail.com

© 2014 Chinese Physical Society and IOP Publishing Ltd

3. Results and discussion

Figure 1(a) shows the optical emission spectra of carbon arc plasmas generated between two graphite electrodes at the ambient pressures of 100 torr, 300 torr, and 500 torr with methane as the feedstock and background gas. The spectra are recorded in the spectral range from 350 nm to 650 nm with an integration time of 300 ms. The plasma temperatures and densities at different CH_4 ambient pressures are determined under the special consideration of local thermodynamic equilibrium (LTE) tested according to McWhirter's criterion.[23] The Boltzmann intensity ratio method and the Saha equation are used respectively to determine the plasma temperature and density with the relative intensities of emitted spectral lines from carbon species in the arc plasma.

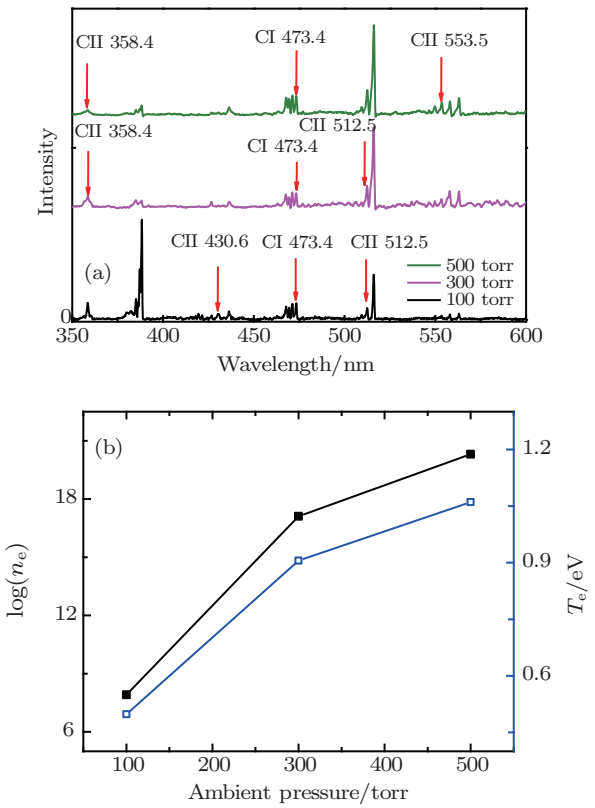


Fig. 1. (color online) (a) Optical emission spectra and (b) electron temperatures and density profiles of the arc plasmas at the pressures of 100 torr, 300 torr, and 500 torr.

Figure 1(b) shows the plasma temperatures and density profiles with respect to the CH_4 ambient pressure. The plasma temperature and density are observed to increase with the increase in the methane ambient pressure, as illustrated in Fig. 1(b).

During the arc discharge, the CH_4 molecules decompose into C and H_2[24] in the plasma region due to the inelastic collisions with electrons, which provides more carbon species within the plasma volume and enhances the Ohmic heating mechanism.[25] The increase in the ambient pressure also confines the plasma in a smaller region and causes the increase of the heat flux at the anode surface, which in turn enhances the ablation at the anode surface. The confinement of the plasma species in a smaller region of the gap between the electrodes leads to the increase in electron temperature and density.[26] The high ambient pressure also causes a change in the electron energy density function, which increases the number of electrons carrying average energy.[27] In the arc discharge plasma, owing to the presence of a strong electric field, the plasma temperature and density are higher along the central line of the discharge and the plasma outflows in the radial direction. During the plasma operation, the partial pressure of the CH_4 molecules decreases due to the dissociation and ionization of the CH_4 molecules. At the same time, the partial pressures of the hydrocarbon molecules C_nH_n ($n = 1, 2, 3, \ldots$) and H_2 molecules increase. A higher concentration of the H_2 gas within the chamber leads to a lower temperature of graphite rods due to their good thermal conductivity. The increase in the chamber pressure also confines the plasma in a small region and leads to the increase of the heat flux at the anode surface which in turn enhances the anode ablation. The confinement of the plasma species in a certain region between the electrodes causes the increase in the plasma temperature and density.[26] However, the plasma temperature and density rising with the increase in the ambient pressure is due to the increase in the decomposition of the CH_4 molecules, which provides more carbon species and confines the arc plasma to a certain region between the electrodes. The closed-end MWCNTs are detected in TEM microscopic analysis along with nanoparticles and amorphous carbon, as shown in Figs. 2 and 3. Figure 2 shows the MWCNTs synthesized at the ambient pressure of 100 torr. The outer and the inner diameters of the observed nanotubes are found to be in the ranges from 7 nm to 20 nm and from 2.5 nm to 5 nm, respectively.

Figure 3 shows the TEM images of grown MWCNTs at the ambient pressure of 500 torr. Highly graphitized MWCNTs with an average tube diameter in the range from 10 nm to 20 nm and an inner diameter less than 1 nm are observed. The surface contamination of the nanotubes with amorphous carbon is also seen with the increase in the CH_4 ambient pressure. The TEM images show that the growth of the carbon nanotube with a smaller inner tube diameter is increased with the increase in the CH_4 ambient pressure from 100 torr to 500 torr. However, at a high ambient pressure of 500 torr, the surface contamination of nanotubes is also enhanced.

Figures 4(a)–4(c) show the scanning electron microscopic images of the MWCNTs synthesized at the ambient pressures 100 torr, 300 torr, and 500 torr, respectively. A high density of MWCNTs along nanoparticles and amorphous carbon can be observed.

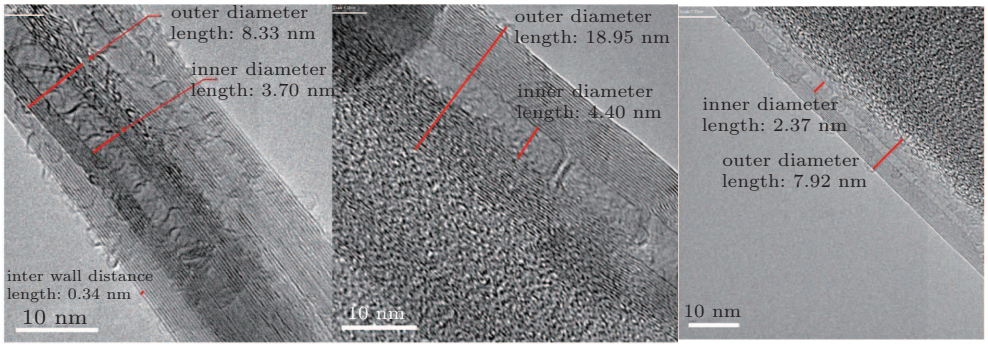


Fig. 2. (color online) TEM images of MWCNTs synthesized with arc current 90 A at ambient pressure 100 torr.

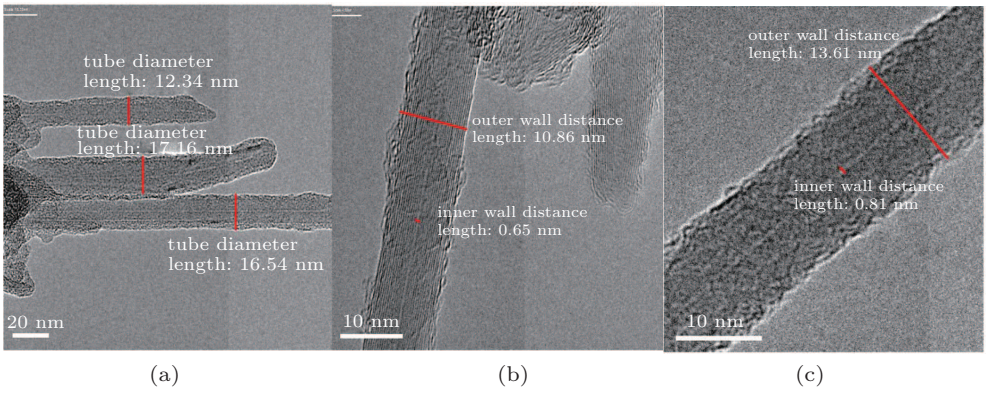


Fig. 3. (color online) TEM images of MWCNTs synthesized with arc current 90 A at ambient pressure 500 torr.

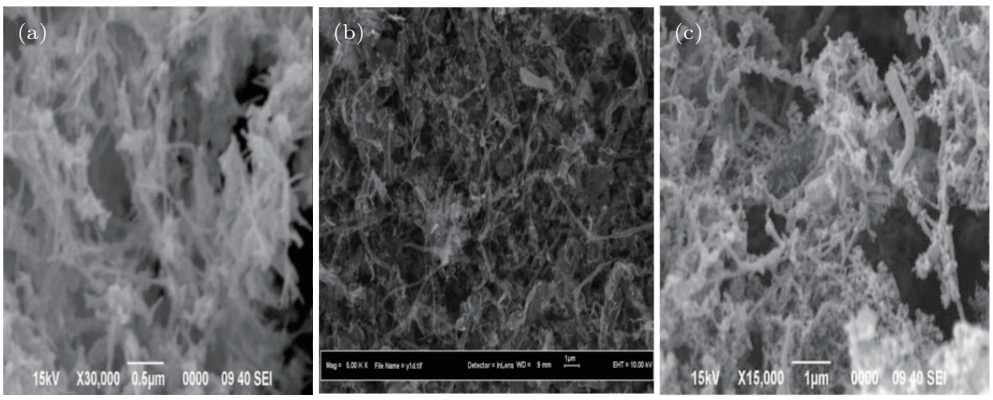


Fig. 4. Scanning electron microscopic images of MWCNTs synthesized at the ambient pressures of (a) 100 torr, (b) 300 torr, and (c) 500 torr.

An increase in the nanotube density is detected with the ambient pressure of CH_4 rising from 100 torr to 500 torr. Beside this, the amorphous carbon and nanoparticles are also observed to increase with ambient pressure increasing. According to the optical emission spectral analysis of the arc plasma, the plasma temperature is observed to rise as the ambient pressure goes up. This shows that the increase in the ambient pressure in turn increases the plasma temperature and density which contributes to the increase in the growth and structural quality of carbon nanotubes and nanostructures. Figure 5 shows the XRD spectra of the MWCNTs synthesized at the ambient pressures of 100 torr, 300 torr, and 500 torr. An intense peak at position $\sim 26.5^\circ$ and several relatively weak peaks at positions $\sim 42.5^\circ$, $\sim 44.5^\circ$, and $\sim 54.5^\circ$ for 2θ associated with graphitic planes (002), (100), (101), and (004)[28] respectively are detected for each recorded XRD spectrum. A prominent increase in the intensity of peak is observed with the increase in the ambient pressure. The peak at position $\sim 26.5^\circ$

corresponds to the (002) graphite plane, which evidences the presence of the graphitized structure.

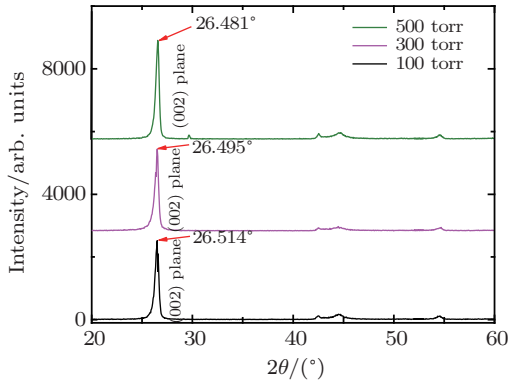


Fig. 5. (color online) XRD spectra of MWCNTs synthesized at the ambient pressures of 100 torr, 300 torr, and 500 torr.

Figures 6(a) and 6(b) show respectively the downshift in angle 2θ and the variation in full width at half maximum (FWHM) for the peak corresponding to the (002) plane with respect to the CH_4 ambient pressure.

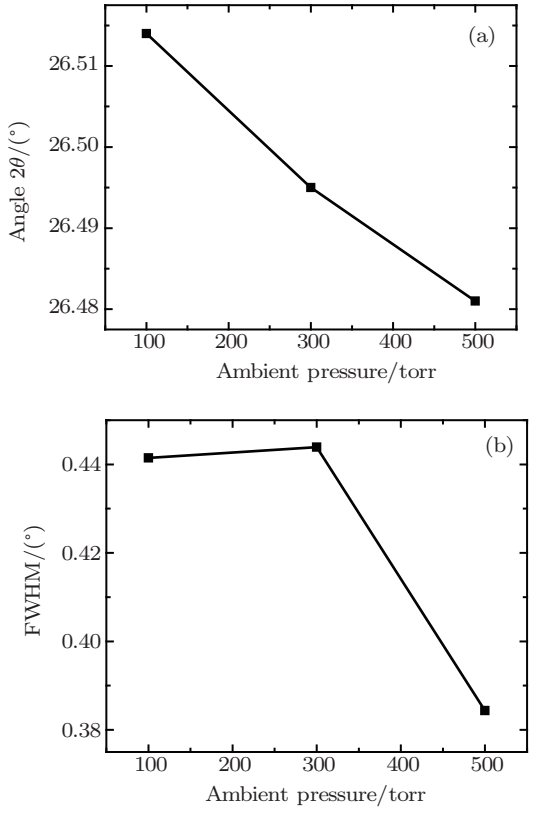


Fig. 6. (a) Angle 2θ and (b) FWHM of the peak associated with the (002) plane of the synthesized MWCNT versus the ambient pressure.

A downshift of the peak associated with the (002) plane towards a low angle is observed with the ambient pressure increasing from 100 torr to 500 torr, as depicted in Fig. 6(a). The peak position shifting towards a lower angle shows that the growth of carbon nanotubes and graphitic nanostructures increases with ambient pressure increasing. The d-spacings in a range from 0.336 nm to 0.340 nm are estimated, which are in agreement with the TEM measurements. An increase in the line width of the (002) peak with the increase in the ambient pressure is observed, as shown in Fig. 6(b). The shift towards a lower angle and broadening in the peak associated with the (002) plane show that the growth of carbon nanotubes and structures increases with the increase in the ambient pressure.

Figure 7 shows the Raman spectra of the MWCNTs synthesized at the ambient pressures of 100 torr, 300 torr, and 500 torr. The spectral lines at positions ~ 1330 cm^{-1}, ~ 1585 cm^{-1}, and ~ 2660 cm^{-1}, called D-line, G-line, and G*-line,[29,30] respectively, are observed. The strong G-lines at position ~ 1585 cm^{-1} in all Raman spectra confirm the presence of carbon nanotubes and graphitic structures in the prepared samples. An increase in the intensity of the G-line is detected with the increase in the ambient pressure, which shows an increase in the MWCNT. The high intensity of the D-line at position ~ 1330 cm^{-1} shows the presence of a poorly-organized graphitic structure. However, the D-line is also considered as an intrinsic feature of the MWCNT Raman spectrum, as the curved nature of the graphite sheets leads to the increase in the intensity of the D-line due to the enhancement in the electron–phonon coupling.[31] The increase in the intensity of the D-line with the increase in the ambient pressure can be ascribed to the presence of defective structures and the increase in the growth of carbon nanotubes with smaller diameters. The position of the D-line in the Raman spectrum strongly depends on laser excitation energy E_{laser}, and the location of the D-line for MWCNT can be expressed as $\omega_{\text{D}} = 1285 + 26.5E_{\text{laser}}$.[31] The Raman analysis shows that E_{laser} is 1.95 eV, thus the position of the D-line should be at 1335 cm^{-1}, which is close to the observed peak in the Raman spectrum.

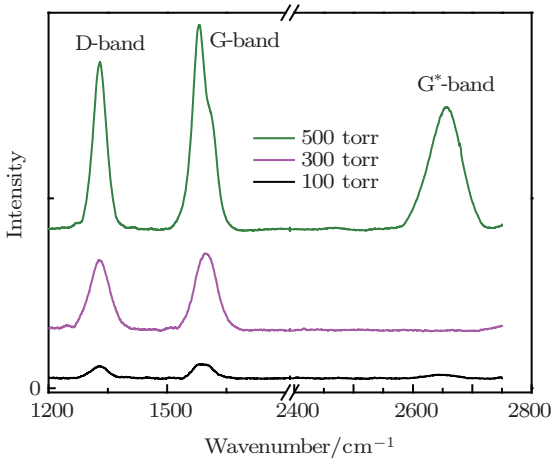


Fig. 7. (color online) Raman spectra of MWCNTs synthesized at pressures of 100 torr, 300 torr, and 500 torr.

The presence of the G*-band shows that the synthesized sample also contains the crystalline graphite in the form of

a monolayer or multilayers of graphene sheets[32] as observed by the TEM microscopy. Thus, the presence of the MWCNT is inferred from the Raman spectra in all the synthesized samples along with graphite crystallites, nanostructures, and graphene. An increase in the relative intensity of the G*-line with the rise in the ambient pressure demonstrates the increase in the growth of graphene stacks.[33]

Figure 8(a) shows the variation in the intensity ratio of D-line to G-line with the ambient pressure. The high I_D/I_G ratios show the presence of disorder structures, amorphous carbon, nanocrystallites, and graphene stacks in the synthesized samples. A first-increase-then-decrease in the I_D/I_G ratio is observed with the increase in the ambient pressures from 100 torr to 300 torr and then to 500 torr. A decrease in the line width of the D-band is seen with the increase in the ambient pressure as shown in Fig. 8(b). From the Raman spectral analysis, it follows that the growth of the graphite crystallite and graphene stacks increases with the increase in the CH_4 pressure.

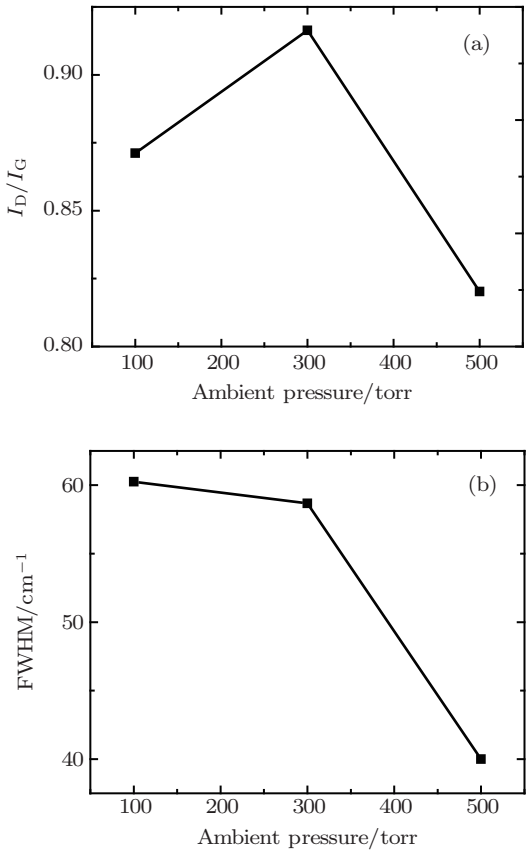


Fig. 8. Variations in (a) I_D/I_G ratio and (b) FWHM of the D-line for the MWCNT versus the ambient pressure.

The FTIR spectra of the MWCNTs synthesized at the pressures of 100 torr, 300 torr, and 500 torr are shown in Fig. 9. The spectral lines in the following ranges: 3740–3840 cm^{-1}, 3400 cm^{-1}, 2920 cm^{-1}, 2850 cm^{-1}, 1630 cm^{-1}, 1560–1580 cm^{-1}, 1420–1460 cm^{-1}, 1380 cm^{-1}, 1160–1170 cm^{-1}, 1110 cm^{-1}, and 1050 cm^{-1} in the FTIR spectra of the synthesized samples are observed. There is no spectral line detected in the range of 1750–2750 cm^{-1}.

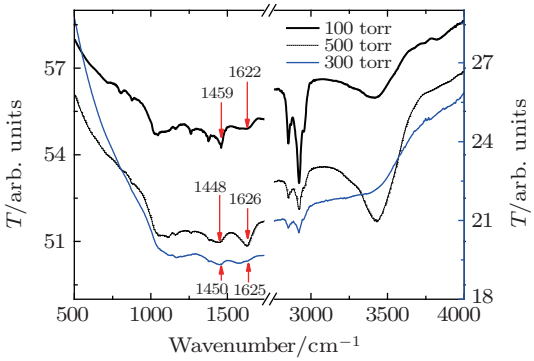


Fig. 9. (color online) FTIR spectra of MWCNTs synthesized at pressures of 100 torr, 300 torr, and 500 torr.

In the FTIR spectra of CNTs, the peaks in the region of 1560–1580 cm^{-1} and at 1460 cm^{-1} represent the C–C vibrational modes associated with the carbon skeleton of the CNTs.[34–37] The peak at $\sim$ 1620 cm^{-1} indicates the presence of the C=C group,[38] which shows the contribution of the sp^3 hybridization.

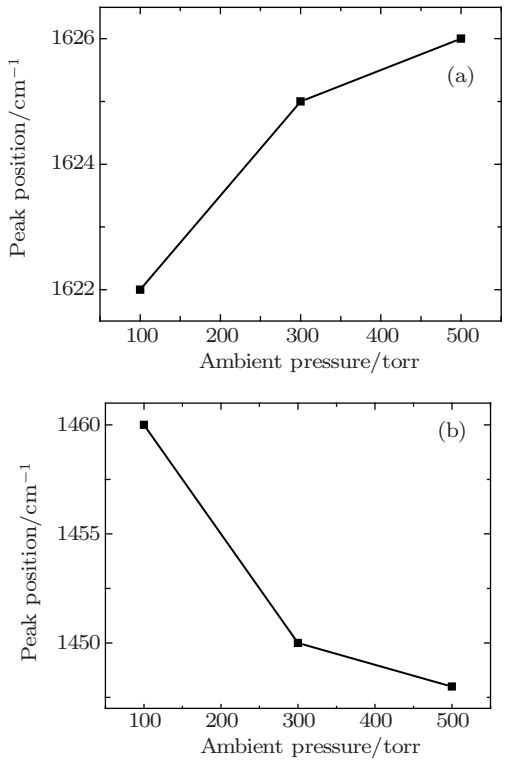


Fig. 10. Shifts of the peaks around (a) 1625 cm^{-1} and (b) 1450 cm^{-1} with the ambient pressure.

The broadening, downshift, and decrease in the height of the peak at position $\sim$ 1625 cm^{-1} associated with the C=C stretching mode are observed with ambient pressure increasing from 100 torr to 500 torr, as shown in Fig. 10(a). However, broadening and a little upshift of the peak at position $\sim$ 1450 cm^{-1} corresponding to the C–C stretching mode are

found with the increase in the ambient pressure, as shown in Fig. 10(b). The downshift and broadening of the peak at position 1630 cm^{-1} indicate the increase in the growth of carbon nanotubes with the increase in the ambient pressure.

4. Conclusion

The MWCNT growth by arc discharge technique is investigated at different ambient pressures of the CH_4 gas. An increase in the plasma temperature and density is found with the increase in the CH_4 ambient pressure. The microscopic, spectroscopic, and XRD analyses of the synthesized MWCNTs show that the increase in the CH_4 ambient pressure leads to the increase in the growth of the MWCNT with a small inner diameter. However, surface contamination and growth of nanoparticles and amorphous carbon also increase at high pressure.

References

[1] Journet C, Picher M and Jourdain V 2012 *Nanotechnology* **23** 142001
[2] Cai X, Cong H and Liu C 2012 *Carbon* **50** 2726
[3] Tam E, Levchenko I, Li J, Shashurin A, Murphy A B, Keidar M and Ostrikov K 2011 *Plasma Science, IEEE Transactions on* **39** 2798
[4] Yong-Bing L, Li S, Chun-Yu Z, Li W, Pan-Ming F, Zhi-Guo Z, Si-Shen X and Guo-Ping W 2005 *Chin. Phys.* **14** 2137
[5] Prasek J, Drbohlavova J, Chomoucka J, Hubalek J, Jasek O, Adam V and Kizek R 2011 *Journal of Materials Chemistry* **21** 15872
[6] Lu B, Huang H, Dong X and Lei J 2010 *J. Phys. D: Appl. Phys.* **43** 105403
[7] Keidar M, Shashurin A, Volotskova O, Raitses Y and Beilis I I 2010 *Phys. Plasmas* **17** 057101
[8] Gu-Ling Z, Jiu-Li W, Xing-Fang W, Wen-Ran F, Guang-Liang C, Wei-Chao G, Er-Wu N, Song-Hua F, Chi-Zi L and Si-Ze Y 2006 *Chin. Phys. Lett.* **23** 1241
[9] Wen-Xia P, Teng L, Xian M, Xi C and Cheng-Kang W 2005 *Chin. Phys. Lett.* **22** 2895
[10] Wei-Dong Y, Pei-Nan W, Zheng-Ping L, Lan M and Fu-Ming L 2002 *Chin. Phys.* **11** 260
[11] Mishra M K, Phukan A and Chakraborty M 2013 *Chin. Phys. Lett.* **30** 015202
[12] Kim Y A, Muramatsu H, Hayashi T and Endo M 2012 *Carbon* **50** 4588
[13] Abdullahi I, Sakulchaicharoen N and Herrera J E 2012 *Diamond and Related Materials* **23** 76
[14] Yan-Hong Y, Run-Cai M, Jin-Tao B and Xun H 2006 *Chin. Phys.* **15** 2761
[15] Wang M, Takegawa H and Saito Y 2004 *Acta Phys. Sin* **53** 888 (in Chinese)
[16] Arepalli S 2004 *Journal of Nanoscience and Nanotechnology* **4** 317
[17] Volotskova O, Levchenko I, Shashurin A, Raitses Y, Ostrikov K and Keidar M 2010 *Nanoscale* **2** 2281
[18] Long Z, Hou-Xian Z, Xuan-Zong Y, Chun-Hua F, Bin Q and Long W 2003 *Chin. Phys. Lett.* **20** 1984
[19] Zhao T 2004 *Acta Phys. Sin.* **53** 3961 (in Chinese)
[20] Kundrapu M, Levchenko I, Ostrikov K and Keidar M 2011 *Plasma Science, IEEE Transactions on* **39** 2876
[21] Scalese S, Scuderi V, Bagiante S, Simone F, Russo P, DUrso L, Compagnini G and Privitera V 2010 *J. Appl. Phys.* **107** 014304
[22] Labedz O, Lange H, Huczko A, Borysiuk J, Szybowicz M and Bystrzejewski M 2009 *Carbon* **47** 2847
[23] Noll R 2012 *Laser-Induced Breakdown Spectroscopy: Fundamentals and Applications* (Berlin: Springer-Verlag)
[24] Shimotani K, Anazawa K, Watanabe H and Shimizu M 2001 *Applied Physics A: Materials Science & Processing* **73** 451
[25] Sharma S and Turner M 2010 *Study of Stochastic Heating in Single Frequency Capacitive Discharges* (Dublin: Ireland)
[26] Tan G and Mieno T 2010 *Jpn. J. Appl. Phys.* **49** 045102
[27] Gordillo-Vázquez F J, Camero M and Gomez-Aleixandre C 2005 *Plasma Sources Science and Technology* **15** 42
[28] Sun Y, Yang S, Sheng G, Guo Z and Wang X 2012 *Journal of Environmental Radioactivity* **105** 40
[29] Belin T and Epron F 2005 *Materials Science and Engineering B* **119** 105
[30] Liang F, Shimizu T, Tanaka M, Choi S and Watanabe T 2012 *Diamond and Related Materials* **30** 70
[31] Sengupta J and Jacob C 2010 *Journal of Nanoparticle Research* **12** 457
[32] Cancado L, Takai K, Enoki T, Endo M, Kim Y, Mizusaki H, Speziali N, Jorio A and Pimenta M 2008 *Carbon* **46** 272
[33] Endo M, Kim Y, Takeda T, Hong S, Matusita T, Hayashi T and Dresselhaus M 2001 *Carbon* **39** 2003
[34] Liu L, Qin Y, Guo Z X and Zhu D 2003 *Carbon* **41** 331
[35] Li Y H, Xu C, Wei B, Zhang X, Zheng M, Wu D and Ajayan P 2002 *Chemistry of Materials* **14** 483
[36] Yan L, Chang P R and Zheng P 2011 *Carbohydrate Polymers* **84** 1378
[37] Naeimi H, Mohajeri A, Moradi L and Rashidi A M 2009 *Applied Surface Science* **256** 631
[38] Sawant S Y, Somani R S, Bajaj H C and Sharma S S 2012 *Journal of Hazardous Materials* **227–228** 317